nature photonics

Article

https://doi.org/10.1038/s41566-022-01120-w

Widely tunable and narrow-linewidth chip-scale lasers from near-ultraviolet to near-infrared wavelengths

Received: 14 September 2021

Accepted: 31 October 2022

Published online: 23 December 2022

Check for updates

Mateus Corato-Zanarella [1] ✉, Andres Gil-Molina [1], Xingchen Ji [2], Min Chul Shin [1], Aseema Mohanty [3] & Michal Lipson [1] ✉

Widely tunable and narrow-linewidth lasers at visible wavelengths are necessary for applications such as quantum optics, optical clocks and atomic and molecular physics. At present, the lasers are benchtop systems, which precludes these technologies from being used outside research laboratories. Here we demonstrate a chip-scale visible laser platform that enables tunable and narrow-linewidth lasers from near-ultraviolet to near-infrared wavelengths. Using micrometre-scale silicon nitride resonators and commercial Fabry–Pérot laser diodes, we achieve coarse tuning up to 12.5 nm and mode-hop-free fine tuning up to 33.9 GHz with intrinsic linewidths down to a few kilohertz. In addition, we show fine-tuning speeds of up to 267 GHz μs^{-1}, fibre-coupled powers of up to 10 mW and typical side-mode suppression ratios above 35 dB. These specifications of our chip-scale lasers have only been achieved previously using large state-of-the-art benchtop laser systems, making our lasers stand out as powerful tools for the next generation of visible-light technologies.

On-chip widely tunable and narrow-linewidth lasers at visible wavelengths are necessary to enable chip-scale technologies for quantum optics[1–3], optical clocks[4,5] and atomic and molecular physics[6–9] (Fig. 1d). A single experiment requires many lasers that emit at different colours to cool, trap and manipulate the species. For example, ^{87}Sr-based optical atomic clocks, which are today's gold standard in clock technology[10,11], can involve lasers that span from near-ultraviolet (near-UV) to near-infrared (near-IR) wavelengths: typically 461 nm and 689 nm for cooling; 813 nm and 914 nm for magic-wavelength trapping; 679 nm and 707 nm for repumping; and 698 nm for clock interrogation, with alternative wavelengths of 497 nm and 520 nm for magic-wavelength trapping; and 403 nm, 481 nm and 497 nm for repumping[12–16]. All of these lasers need to be precisely tunable and have submegahertz intrinsic linewidths to address specific atomic transitions. At present, the lasers used are benchtop systems and are predominantly based on semiconductor diode lasers such as Fabry–Pérot (FP) laser diodes. Since FP laser diodes are not single frequency, external free-space cavities are used to make them narrow linewidth and tunable via self-injection locking. However, to take quantum optics experiments and atomic clocks outside research laboratories, these laser sources need to be compact. Centimetre-scale lasers based on whispering gallery mode resonators as external cavities have been shown for wavelengths around 780 nm (ref. 17), 492 nm (ref. 18), 447 nm (ref. 19) and 370 nm (ref. 20), although they have restricted tunability and require free-space components. Recently, Franken et al.[21] demonstrated a chip-scale laser based on a low-confinement silicon nitride (Si_3N_4) chip, but only in the red spectral range (684 nm) and with tunability restricted to a low optical power (0.4 mW).

Here we demonstrate a chip-scale laser platform that enables wide-tunability, narrow-linewidth and robust lasing from near-UV (404 nm) to near-IR (785 nm) wavelengths (Fig. 1a). Our platform uses tightly confined, micrometre-scale Si_3N_4 resonators with high

[1]Department of Electrical Engineering, Columbia University, New York, NY, USA. [2]John Hopcroft Center for Computer Science, Shanghai Jiao Tong University, Shanghai, China. [3]Department of Electrical and Computer Engineering, Tufts University, Medford, MA, USA. ✉e-mail: mcz2109@columbia.edu; ml3745@columbia.edu

https://doi.org/10.1038/s41566-022-01120-w

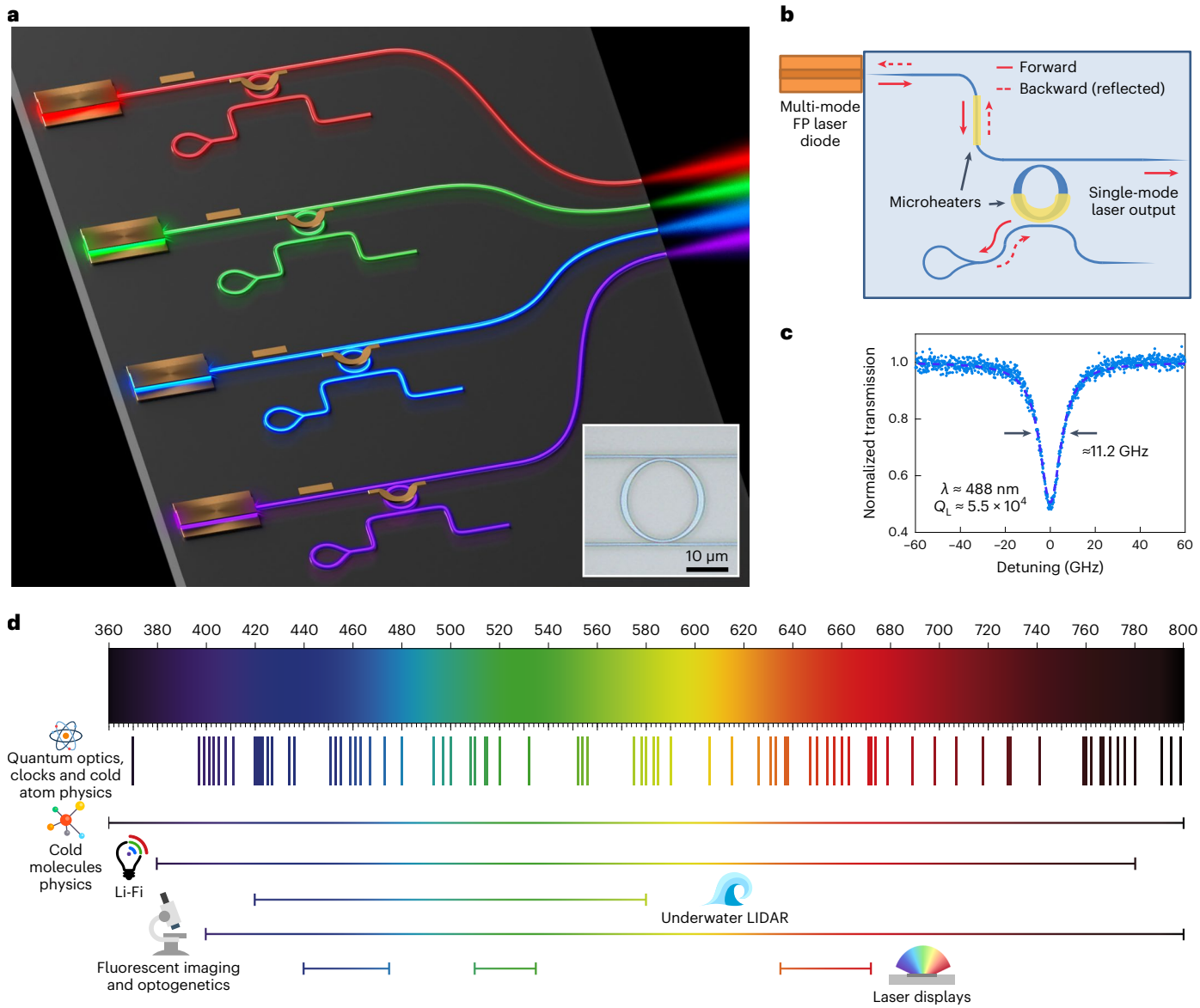

Fig. 1 | Chip-scale, multi-wavelength visible lasers and applications of visible light. a, Vision of our integrated platform, where a single chip generates narrow-linewidth and tunable visible light that covers all colours. Inset: Microscope image of the ring resonator before microheater deposition. We make the waveguides using 175-nm-thick Si_3N_4 surrounded by SiO_2 (see Methods for fabrication details). The ring has a bending radius of 10 μm and a width that increases from 300 nm at the coupling regions to 1,500 nm in between. The large FSR prevents mode-hopping, and the tapering of the width ensures single-mode operation with a high Q value despite the small footprint. **b**, Schematic of an integrated visible laser using our platform. We edge couple an FP laser diode that emits light of the desired colour to the Si_3N_4 chip. We use a ring resonator with a feedback loop at the drop port to reflect part of the resonant light back to the FP laser, which leads to self-injection locking. We select the lasing wavelength using phase shifters (microheaters) on top of the ring resonator and the bus waveguide. **c**, Example of ring resonance measured in blue (wavelength, λ, around 488 nm). The loaded quality factor, Q_L, is 5.5×10^4 with an extinction ratio of 50%. We provide resonance measurements at other wavelengths and an analysis of the loss and operation of the resonators in Supplementary Section 1.1. **d**, Notable applications of visible-light lasers. The wide range of technologies that use light from the near-UV to near-IR regions include quantum optics, optical clocks, atomic and molecular physics, visible-light communications (Li-Fi), underwater ranging, biophotonics and laser displays. We list the articles referenced for preparing this schematic in Supplementary Section 5. We also provide an extended version of the portion 'Quantum optics, clocks and cold atoms physics' of this panel with a list of the species corresponding to each line in Supplementary Section 5. Quantum optics and cold molecules physics icons in **d** reproduced with permission under a Creative Commons license CC0. Li-Fi, fluorescent imaging and underwater LIDAR icons in **d** adapted with permission under a Creative Commons license CC0.

quality factor (Q), and hybrid integration of commercial FP laser diodes (Fig. 1b). We achieve tunable and narrow-linewidth lasing across the visible spectrum by designing a broadband and low-loss optical-feedback scheme based on ring resonators. We leverage the high confinement to make the resonators small, with a 10 μm bending radius (Fig. 1a inset). The resulting large free spectral range (FSR) of several nanometres for all wavelengths (Supplementary Section 1.1) ensures mode-hop-free operation with a high side-mode suppression ratio (SMSR) by suppressing mode competition via selective feedback to a single longitudinal mode of the FP laser diode. In contrast to using Vernier filters[21], our approach requires fewer phase shifters, thus eliminating unnecessary noise and thermal crosstalk, reducing power consumption and enabling a small footprint. The low loss and tunability of the rings using the microheaters translate into the narrow-linewidth and tunable laser

https://doi.org/10.1038/s41566-022-01120-w

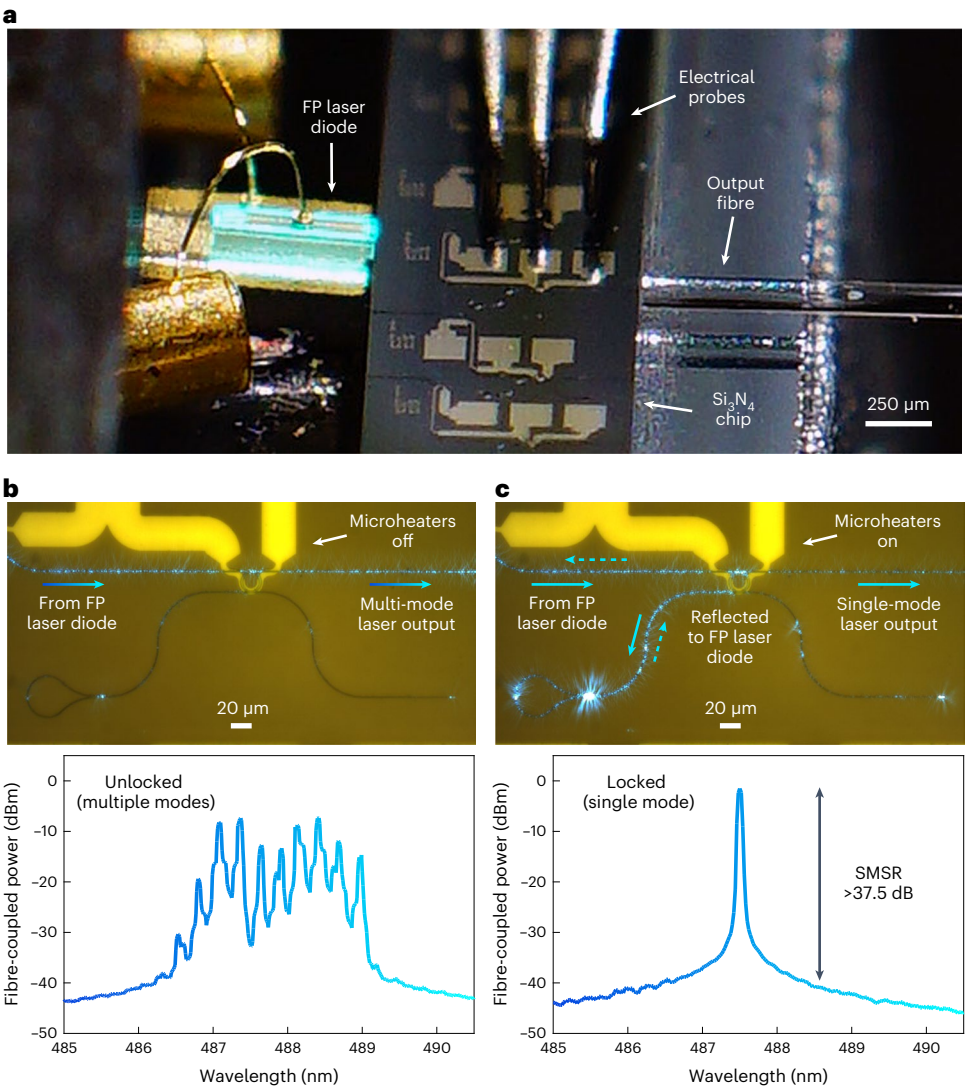

Fig. 2 | Example of chip-scale laser (blue wavelength range) and its operation. **a**, Photo of the chip-scale blue laser. We edge couple the FP laser diode to the Si_3N_4 chip and collect the output with a cleaved fibre. We drive the thermo-optic phase shifters using electrical probes. **b**, Ring resonance is detuned from the FP laser diode modes, resulting in no light in the feedback loop (top). The chip output resembles the usual output of the FP laser with multiple lasing modes (bottom). **c**, We tune the ring resonance to one of the FP modes, making the feedback loop reflect part of the light back to the diode (top). Self-injection locking causes all the longitudinal modes to collapse into a single-frequency, narrow-linewidth lasing mode with a high (>37.5 dB) SMSR (bottom). The optical spectra are measured using an optical spectrum analyser (resolution, 0.05 nm). We show photos of the chip-scale lasers operating in the other spectral ranges in Supplementary Section 2.6. We also provide a detailed analysis of the self-injection locking process in Supplementary Section 2.2.

light. In contrast to typical low-loss resonators with orders of magnitude larger radii[21–24] (Supplementary Section 1.1), we simultaneously realize compact and low-loss single-mode operation by tapering the ring width from 1,500 nm to 300 nm (Fig. 1a inset and 1c)[25–27]. We use the highly multi-mode cross-sections (up to 1,500 nm) to reduce the overlap between the optical mode and the waveguide sidewalls[28], which is critical for broadband low loss since surface scattering increases drastically at visible wavelengths[29]. At the coupling regions, we taper the width to 300 nm to ensure the excitation and propagation of only the fundamental mode, which is important for preventing undesired optical feedback from higher order modes. The narrow width also provides broadband strong coupling between the waveguides and the ring by increasing their modal overlaps, ensuring that enough power is dropped to the feedback loop and is reflected back to the FP laser diodes to cause self-injection locking.

We choose FP laser diodes as the light sources to leverage their robust self-injection locking against coupling loss and unwanted reflections[30]. Our system ensures robustness by keeping the main laser cavity formed by the FP laser facets separate from the photonic chip, whose role is just to collapse the multi-mode emission of the FP laser into a narrow and tunable single-frequency line via self-injection locking[30–32]. This is in contrast to lasers based on reflective semiconductor optical amplifiers, in which the photonic chip and its interface are part of the lasing cavity. Any loss or reflection leads to a strong impact on the lasing dynamics, in particular at powers far above the threshold, which has limited visible lasers based on reflective semiconductor optical amplifiers to the red spectral range and with tunability only at low optical power values (0.4 mW)[21]. By leveraging the robustness and scalability of our FP laser-based scheme, we enable stable and tunable lasing from near-UV to near-IR wavelengths in a photonic integrated platform.

We collapse the longitudinal modes of the edge-coupled FP laser diodes (Fig. 2a) into single-frequency lines via independent phase control of the bus waveguide and ring resonator. We use the ring

https://doi.org/10.1038/s41566-022-01120-w

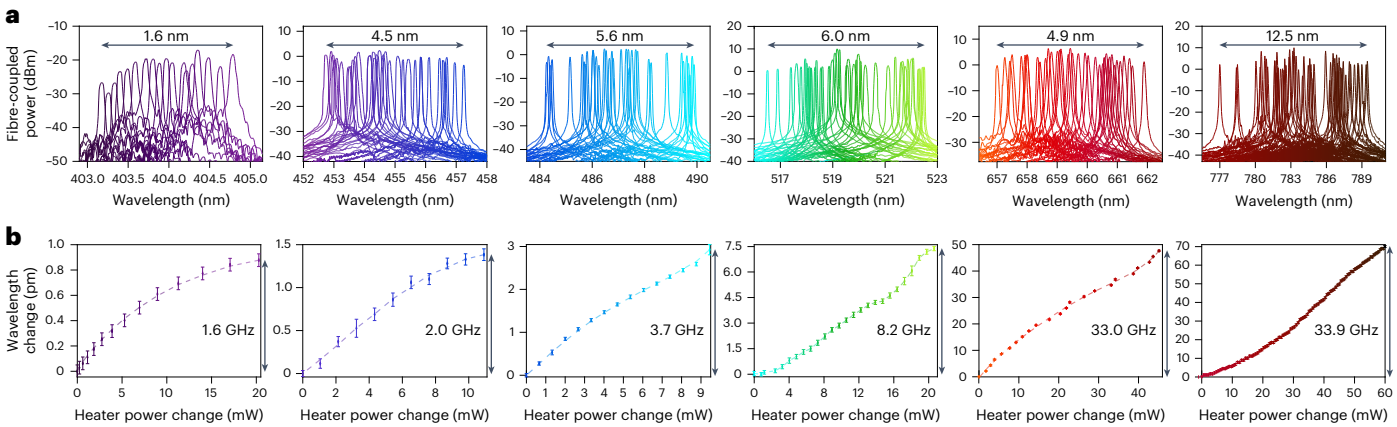

Fig. 3 | Coarse and fine wavelength tuning of the chip-scale lasers from near-UV to near-IR wavelengths. a, Coarse-tuning ranges at (from left to right) near-UV, deep-blue, blue, green, red and near-IR wavelengths. We achieve coarse tuning by controlling the on-chip phase shifters while keeping the current and temperature of the FP laser diodes fixed. We measure the optical spectra using an optical spectrum analyser (resolution, 0.05 nm) and overlay them to depict the tuning ranges. **b**, Mode-hop-free fine tuning (frequency pulling) as a function of the power applied to the ring microheater at the same wavelength ranges (mean ± s.d.; see Supplementary Section 2.7). We achieve fine tuning by changing the power applied to the ring microheater after self-injection locking of the laser. We measure the detuning from the initial wavelength using a wavemeter (see Methods). We present the detailed characteristics of the FP laser diodes and the chip-scale lasers, such as light–current–voltage curves, beam profiles and operating conditions, in Supplementary Section 2.

phase shifter to control the wavelength of the reflected light, and the bus phase shifter to adjust its phase. When we detune the resonator from the modes of the FP laser, the ring is decoupled from the system (Fig. 2b, top) and the FP diode lases with multiple longitudinal modes (Fig. 2b, bottom). When we align the ring resonance to a mode of the FP laser, some of its optical power is reflected back to the diode (Fig. 2c, top). When we further adjust the phase of the reflected light via the bus phase shifter to ensure its constructive interference with the light inside the FP laser, self-injection locking occurs and converts the output of the chip into a single-frequency laser with a narrow linewidth (Fig. 2c, bottom). This self-injection locking phenomenon has been traditionally used in free-space external-cavity diode lasers and was recently brought to the context of integrated photonics in the infrared spectral range, where it has enabled ultranarrow-linewidth, tunable lasers and fully integrated frequency comb generation[30,33–38]. We coarsely tune the wavelength of our chip-scale lasers by aligning the ring resonance to different longitudinal modes of the FP laser. We fine tune the wavelength in between FP modes via frequency pulling[30,31] by tuning the ring resonance when the laser is locked, which changes the frequency of the optical feedback and consequently the lasing wavelength. Throughout the frequency-pulling process, we keep the bus phase shifter constant. Alternatively, we also achieve frequency pulling by changing the FP laser current while keeping the ring resonance fixed[17–20].

Results

We demonstrate tunable lasing in the near-UV (404 nm), deep-blue (450 nm), blue (488 nm), green (520 nm), red (660 nm) and near-IR (785 nm) wavelength ranges, with coarse tuning up to 12.5 nm and mode-hop-free fine tuning up to 33.9 GHz (Fig. 3). In addition, we achieve fibre-coupled powers of up to 10 mW and typical SMSRs above 35 dB (Supplementary Section 2.6) with stable mode-hop-free operation up to 5.7 h, limited only by the coupling-stage drift (Supplementary Section 2.8). To characterize our chip-scale lasers, we collect the chip output using edge-coupled cleaved fibres (Fig. 2a and Supplementary Section 1.3). We observe a reduction in the threshold current of the chip-scale lasers compared with the free-running FP laser diodes, which is a characteristic signature of self-injection locking[39–42] (Supplementary Section 2.3). We measure the coarse-tuning ranges from 1.6 nm to 12.5 nm (Fig. 3a) limited by the gain bandwidth of the FP laser diodes, and the mode-hop-free fine-tuning ranges from 1.6 GHz to 33.9 GHz (Fig. 3b) (Supplementary Section 2.7). We summarize the tuning ranges, fibre-coupled powers and SMSRs of all the chip-scale lasers in Table 1. We obtain the coarse-tuning ranges by overlapping the chip's output spectra acquired using an optical spectrum analyser for different self-injection locked wavelengths. We measure the mode-hop-free fine-tuning ranges by changing the power applied to the ring microheater while monitoring the lasing wavelength with a wavemeter (Supplementary Section 2.7) after self-injection locking of the lasers. For our chip-scale lasers, the wide tunability of many nanometres, the large mode-hop-free tuning ranges of up to tens of gigahertz and the fibre-coupled output power levels of several milliwatts are paralleled only by state-of-the-art benchtop laser systems (Supplementary Section 4).

We show fine-tuning speeds of up to 7 GHz μs^{-1} via modulation of the ring microheater (Fig. 4a) and up to 267 GHz μs^{-1} via modulation of the FP laser current (Fig. 4b), the latter being limited only by our experimental setup. We characterize the microheater-based frequency tuning speeds by scanning a fixed FP interferometer and we measure a 3 dB modulation bandwidth of around 32 kHz across the whole visible spectrum (Supplementary Section 2.9.1). The fast and long-range tuning (up to tens of gigahertz) that is enabled by our microheaters makes our lasers ideal for applications such as in swept-wavelength spectroscopy[43] and frequency-modulated continuous-wave LIDAR (light detection and ranging)[36,37,44]. We characterize the FP laser-current modulation by beating the chip-scale laser output to a commercial laser and we apply modulation frequencies of up to 20 MHz (Supplementary Section 2.9.2), limited only by our experimental setup. The ultrafast and short-range tuning (up to several gigahertz) that is enabled by the current modulation is crucial for laser frequency stabilization and linewidth narrowing via negative electronic feedback[38,45,46]. Our tuning speeds are faster than the specifications of state-of-the-art commercial laser systems (≤0.02 GHz μs^{-1} for piezo tuning; Supplementary Section 4.2) and of integrated or partially integrated visible lasers (≤4.1×10^{-7} GHz μs^{-1}; Supplementary Section 4.1).

We measure the linewidths of the chip-scale lasers and obtain intrinsic linewidths ranging from <8 kHz to <26 kHz from deep-blue to near-IR regions and an effective linewidth of <3.3 MHz for the near-UV region, which are all upper bounds limited by our instruments (Table 1). We determine the linewidths from deep-blue to near-IR wavelengths

https://doi.org/10.1038/s41566-022-01120-w

Table 1 | Summary of the specifications of our chip-scale visible lasers from near-UV to near-IR wavelengths

Centre wavelength (nm)	Coarse-tuning range (nm)	Mode-hop-free fine-tuning range (GHz)	Fine-tuning rate (GHz μs^{-1})	Fine-tuning 3 dB modulation bandwidth	Measured intrinsic linewidth (kHz)	Measured effective linewidth (kHz)	Estimated intrinsic linewidth (kHz)	SMSR (dB)	Fibre-coupled output power (mW)	Estimated on-chip power (mW)[a]	Approximate footprint (FP laser diode+photonic chip) (mm^2)
785	12.5	33.9	7.1 (microheater) 267 (laser current)[b]	34 kHz (microheater) >20 MHz (laser current)[b]	<9[b]	<359[b]	<1.1	≥37	10.00	11.24	0.6×2
660	4.9	33.0	3.4 (microheater)	31 kHz (microheater)	<10[b]	<427[b]	<1.4	≥35	4.42	7.13	0.6×2
520	6.0	8.2	N/A	32 kHz (microheater)	<26[b]	<373[b]	<0.4	≥37	9.89	10.75	0.6×2
488	5.6	3.7	N/A	31 kHz (microheater)	<8[b]	<505[b]	<1.4	≥37	1.75	8.33	0.6×2
455	4.5	2.0	N/A	32 kHz (microheater)	<9[b]	<374[b]	<6.9	≥37	1.74	5.61	0.6×2
404	1.6	1.6	N/A	N/A	N/A	<3,300[b]	<1,500	≥21	0.02	0.13	0.6×2

We keep the FP laser diodes at room temperature and drive them using a constant pump current, except for the linewidth measurements for 660 nm and 455 nm, which required a change in temperature, and the laser-current-based tuning rate, where we modulate the current around its nominal value (Supplementary Section 2.5). We present a comparison with the specifications of other laser systems in Supplementary Section 4. [a]Estimated using the coupling losses from Supplementary Section 1.3 (Supplementary Table 1). [b]Limited by the measurements.

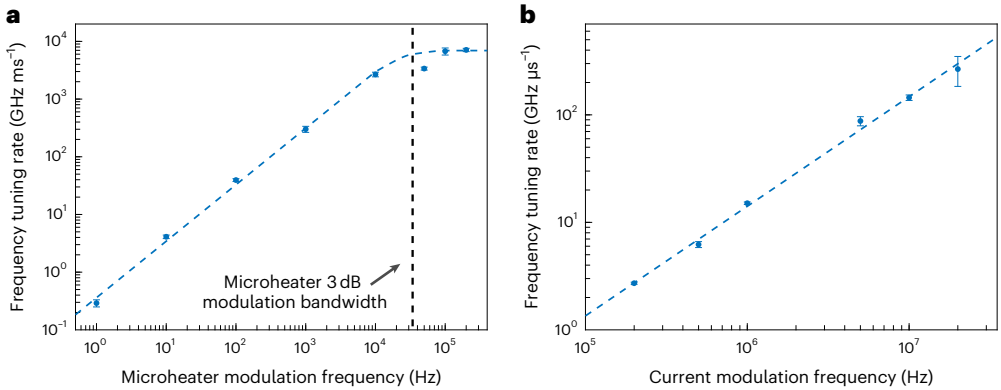

Fig. 4 | Fine frequency tuning speeds via microheater and laser-current modulations. a, Frequency tuning rate as a function of the microheater driving frequency for the near-IR chip-scale laser, showing tuning rates of up to 7 GHz μs^{-1} with a modulation bandwidth of 34.1 ± 0.3 kHz. The relationship is mostly linear for frequencies below the 3 dB modulation bandwidth of the microheater (black dashed line) and saturates above it. We present similar results for the red chip-scale laser, with tuning rates of up to 3.4 GHz μs^{-1} and a modulation bandwidth of 31.1 ± 0.2 kHz, in Supplementary Section 2.9.1.2. Since the maximum tuning rate is limited by the microheater's frequency response that is wavelength-insensitive (Supplementary Section 2.9.1.2), we expect a similar performance for all the chip-scale lasers. **b**, Frequency tuning rate as a function of the FP laser-current driving frequency for the near-IR chip-scale laser, showing tuning rates of up to 267 GHz μs^{-1} for modulation frequencies up to 20 MHz, limited only by our experimental setup. The relationship is mostly linear throughout, and we expect that the laser current can be modulated with frequencies of up to several gigahertz (ref. 60). Since the maximum laser-current-based tuning rate is limited by the FP laser's frequency response and it is similar for FP lasers across the visible spectrum[39] (Supplementary Sections 2.9.2 and 4), we expect a similar performance for all the chip-scale lasers. Throughout, the error bars correspond to the mean ± s.d. of 50 consecutive measurements, and the blue dashed lines are to guide the eye. We present the supporting data for the plots and detailed descriptions of the measurements in Supplementary Section 2.9.

by measuring the heterodyne beat note between our chip-scale lasers and commercial narrow-linewidth laser systems using a spectrum analyser (Supplementary Section 2.10). We fit the beat notes using a Voigt profile and extract both the Lorentzian contribution, which corresponds to the white noise that defines the intrinsic linewidth, as well as the Gaussian contribution, which corresponds to the flicker and technical noises that broaden the effective linewidth[47]. We also extract the effective 3 dB linewidths of the lasers, which are represented by the total Voigt linewidths (Supplementary Section 2.12). For the linewidth measurements in the deep-blue and red spectral ranges, we change the temperature of the FP lasers to above and below room temperature, respectively, to spectrally shift the centre wavelengths of our chip-scale lasers to overlap with the tuning ranges of the commercial lasers (Supplementary Sections 2.10 and 3). Since the commercial laser systems have intrinsic linewidths of several kilohertz and effective linewidths of hundreds of kilohertz (Supplementary Section 3), we conclude that the beat notes are limited by their linewidths. For the near-IR chip-scale laser, we confirm this via a direct measurement of its frequency noise using a linewidth analyser, which suggests an intrinsic linewidth of between 314 Hz and 1.26 kHz (Supplementary Section 2.11). We determine the effective linewidth of the near-UV laser to be <3.3 MHz by scanning it with an FP interferometer with a limited resolution of 2.5 MHz (Supplementary Section 2.10). We theoretically estimate the intrinsic linewidths of the chip-scale lasers to be <7 kHz from deep-blue to near-IR regions and <1.5 MHz for near-UV wavelengths (Table 1 and Supplementary Section 2.13), further supporting the experimental results in Fig. 5 and indicating that they are probably limited by our instruments. Our demonstrated linewidths are comparable

https://doi.org/10.1038/s41566-022-01120-w

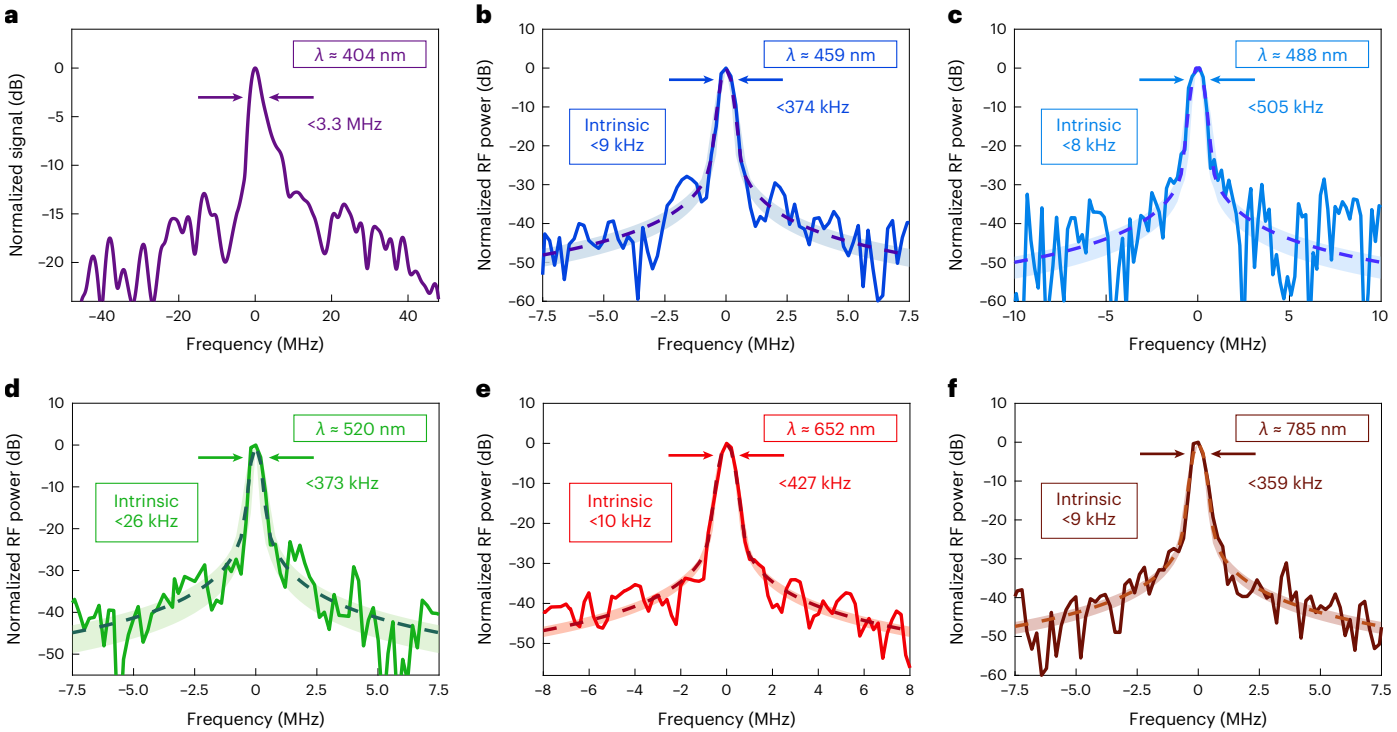

Fig. 5 | Linewidth measurements of the chip-scale lasers from near-UV to near-IR wavelengths. a, Estimated lineshape of the near-UV laser measured with a scanning FP interferometer. The effective linewidth of <3.3 MHz is an upper bound due to measurement-induced broadening (Supplementary Section 2.10). **b**–**f**, Heterodyne beat notes between our deep-blue (**b**), blue (**c**), green (**d**), red (**e**) and near-IR (**f**) chip-scale lasers and commercial narrow-linewidth laser systems. Since the commercial laser systems have intrinsic linewidths of several kilohertz and effective linewidths of hundreds of kilohertz (Supplementary Section 3), we conclude that the beat notes are limited by their linewidths. The shaded areas correspond to the 95% confidence interval of the Voigt fittings (dashed lines), and the reported linewidths are their upper bounds. The arrows indicate the 3 dB level of the effective linewidth. We summarize the fitted linewidths and their confidence intervals in Supplementary Table 3 of Supplementary Section 2.10. We measure the beat notes using a spectrum analyser (Agilent E4407B) with a sweep time of 4.99 ms, a resolution bandwidth of 30 kHz and a scanning window of 100 MHz around the beat note. RF, radio frequency.

to state-of-the-art narrow-linewidth and tunable visible lasers (Supplementary Section 4), which are typically benchtop systems that are bulky.

Discussion

Our chip-scale visible lasers exhibit high performance in the key specifications of the tuning range, tuning speed, linewidth, power and SMSR, which were previously only achieved using benchtop laser systems. Our platform does not require free-space optical components, has a micrometre-scale footprint and works robustly across almost an octave. Owing to its small footprint and broadband operation, our platform is easily scalable and enables multiple lasers of different wavelengths to be integrated on the same chip[48,49]. If a single-fibre output is desired, all the different colours can be combined into a regular or photonic crystal single-mode fibre[50] using an on-chip wavelength multiplexer[51]. Such a compact and highly coherent multi-colour laser engine is critical for quantum optics, atomic clocks, atomic and molecular physics, biophotonics, augmented reality/virtual reality, spectroscopy and visible-light communications. By independently controlling the on-chip microheaters, laser current and laser temperature, we can align the ring resonance and the FP longitudinal modes at any desired wavelength, enabling precise and gap-free tuning[52,53] over wide spectral ranges of several nanometres across the visible spectrum. Moreover, we can extend the coarse-tuning ranges by several nanometres towards both longer and shorter wavelengths by changing the temperature of the FP lasers, as demonstrated by the linewidth measurements in the deep-blue and red regions (Fig. 5 and Supplementary Section 2.10). We can also widen the frequency-pulling ranges by driving the microheaters and the laser current in a feed-forward fashion[41,54,55]. The overall performance of our lasers, in particular the frequency-pulling ranges and the output powers, are currently limited only by the coupling losses between the FP lasers and the photonic chip, which determine the strength of the self-injection locking via the amount of reflected light[31]. By optimizing the couplings, one can further improve the specifications of the lasers, particularly at the near-UV spectral range where the coupling losses are currently higher (Supplementary Sections 1.3 and 2.13). In addition to our tapering strategy, compact and low-loss resonators with single-mode operation may potentially be achieved by employing adiabatic coupling schemes to rings with constant multi-mode cross-sections, as has been investigated at infrared wavelengths[56,57]. The self-injection locking robustness can enable scaling to even higher on-chip power levels[58] using commercial high-power (>1 W) visible-light laser diodes, opening the door to fully integrated high-power sources for nonlinear optics and optical cooling and trapping. The wafer-scale Si_3N_4 platform is currently available in photonic foundries, enabling inexpensive mass production and large-scale deployment. These unique features of our chip-scale platform break the existing paradigm in which high-performance visible lasers require discrete benchtop components, paving the way for fully integrated visible-light systems for applications in the life sciences, atomic research and vision sciences.

Note added in proof

While this article was under review, Siddharth et al.[59] showed lasers at visible wavelengths using a low-confinement Si_3N_4 chip, but with restricted tunability and a greater than megahertz intrinsic linewidth

that was only measured at 461 nm. We present a quantitative comparison with our work in Supplementary Section 4.1.3.

Online content

Any methods, additional references, Nature Portfolio reporting summaries, source data, extended data, supplementary information, acknowledgements, peer review information; details of author contributions and competing interests; and statements of data and code availability are available at https://doi.org/10.1038/s41566-022-01120-w.

References

1. Niffenegger, R. J. et al. Integrated multi-wavelength control of an ion qubit. *Nature* **586**, 538–542 (2020).
2. Moody, G. et al. Roadmap on integrated quantum photonics. *JPhys. Photonics* **4**, 012501 (2022).
3. Mehta, K. K. et al. Integrated optical multi-ion quantum logic. *Nature* **586**, 533–537 (2020).
4. Kómár, P. et al. A quantum network of clocks. *Nat. Phys.* **10**, 582–587 (2014).
5. Nichol, B. C. et al. An elementary quantum network of entangled optical atomic clocks. *Nature* **609**, 689–694 (2022).
6. Tomza, M. et al. Cold hybrid ion–atom systems. *Rev. Mod. Phys.* **91**, 035001 (2019).
7. Gross, C. & Bloch, I. Quantum simulations with ultracold atoms in optical lattices. *Science* **357**, 995–1001 (2017).
8. Mitra, D., Leung, K. H. & Zelevinsky, T. Quantum control of molecules for fundamental physics. *Phys. Rev. A* **105**, 040101 (2022).
9. Will, S. et al. Time-resolved observation of coherent multi-body interactions in quantum phase revivals. *Nature* **465**, 197–201 (2010).
10. Campbell, S. L. et al. A Fermi-degenerate three-dimensional optical lattice clock. *Science* **358**, 90–94 (2017).
11. Oelker, E. et al. Demonstration of 4.8×10^{-17} stability at 1 s for two independent optical clocks. *Nat. Photonics* **13**, 714–719 (2019).
12. Moriya, P. H. et al. Comparison between 403 nm and 497 nm repumping schemes for strontium magneto-optical traps. *J. Phys. Commun.* **2**, 125008 (2018).
13. Ding, R. et al. Creation of vibrationally-excited ultralong-range Rydberg molecules in polarized and unpolarized cold gases of ^{87}Sr. *J. Phys. B* **53**, 014002 (2019).
14. Young, A. W. et al. Half-minute-scale atomic coherence and high relative stability in a tweezer clock. *Nature* **588**, 408–413 (2020).
15. Bowden, W. et al. A pyramid MOT with integrated optical cavities as a cold atom platform for an optical lattice clock. *Sci. Rep.* **9**, 11704 (2019).
16. Bongs, K. et al. Development of a strontium optical lattice clock for the SOC mission on the ISS. *C. R. Phys.* **16**, 553–564 (2015).
17. Lai, Y.-H. et al. 780 nm narrow-linewidth self-injection-locked WGM lasers. *Proc. SPIE* **11266**, 112660O (2020).
18. Savchenkov, A. A. et al. Application of a self-injection locked cyan laser for barium ion cooling and spectroscopy. *Sci. Rep.* **10**, 16494 (2020).
19. Donvalkar, P. S., Savchenkov, A. & Matsko, A. Self-injection locked blue laser. *J. Opt.* **20**, 045801 (2018).
20. Savchenkov, A. A. et al. Self-injection locking efficiency of a UV Fabry–Perot laser diode. *Opt. Lett.* **44**, 4175–4178 (2019).
21. Franken, C. A. A. et al. Hybrid-integrated diode laser in the visible spectral range. *Opt. Lett.* **46**, 4904–4907 (2021).
22. Chauhan, N. et al. Ultra-low loss visible light waveguides for integrated atomic, molecular, and quantum photonics. *Opt. Express* **30**, 6960–6969 (2022).
23. Chauhan, N. et al. Visible light photonic integrated Brillouin laser. *Nat. Commun.* **12**, 4685 (2021).
24. Morin, T. J. et al. CMOS-foundry-based blue and violet photonics. *Optica* **8**, 755–756 (2021).
25. Corato-Zanarella, M. et al. Overcoming the trade-off between loss and dispersion in microresonators. In *Conference on Lasers and Electro-Optics* paper STh1J.1 (Optica Publishing Group, 2020); https://doi.org/10.1364/CLEO_SI.2020.STh1J.1
26. Liang, G. et al. Robust, efficient, micrometre-scale phase modulators at visible wavelengths. *Nat. Photonics* **15**, 908–913 (2021).
27. Li, X., Deng, Q. & Zhou, Z. Low loss, high-speed single-mode half-disk resonator. *Opt. Lett.* **39**, 3810–3813 (2014).
28. Ji, X. et al. Ultra-low-loss on-chip resonators with sub-milliwatt parametric oscillation threshold. *Optica* **4**, 619–624 (2017).
29. Payne, F. P. & Lacey, J. P. R. A theoretical analysis of scattering loss from planar optical waveguides. *Opt. Quantum Electron.* **26**, 977–986 (1994).
30. Gil-Molina, A. et al. Robust hybrid III-V/Si_3N_4 laser with kHz-linewidth and GHz-pulling range. In *Conference on Lasers and Electro-Optics* paper STu3M.4 (Optica Publishing Group, 2020); https://doi.org/10.1364/CLEO_SI.2020.STu3M.4
31. Kondratiev, N. M. et al. Self-injection locking of a laser diode to a high-Q WGM microresonator. *Opt. Express* **25**, 28167–28178 (2017).
32. Galiev, R. R. et al. Spectrum collapse, narrow linewidth, and Bogatov effect in diode lasers locked to high-Q optical microresonators. *Opt. Express* **26**, 30509–30522 (2018).
33. Raja, A. S. et al. Electrically pumped photonic integrated soliton microcomb. *Nat. Commun.* **10**, 680 (2019).
34. Li, B. et al. Reaching fiber-laser coherence in integrated photonics. *Opt. Lett.* **46**, 5201–5204 (2021).
35. Xiang, C. et al. Laser soliton microcombs heterogeneously integrated on silicon. *Science* **373**, 99–103 (2021).
36. Snigirev, V. et al. Ultrafast tunable lasers using lithium niobate integrated photonics. Preprint at https://arxiv.org/abs/2112.02036 (2022).
37. Lihachev, G. et al. Low-noise frequency-agile photonic integrated lasers for coherent ranging. *Nat. Commun.* **13**, 3522 (2022).
38. Guo, J. et al. Chip-based laser with 1-hertz integrated linewidth. *Sci. Adv.* **8**, eabp9006 (2022).
39. Shamim, M. H. M. et al. Investigation of self-injection locked visible laser diodes for high bit-rate visible light communication. *IEEE Photonics J.* **10**, 7905611 (2018).
40. Shamim, M. H. M., Ng, T. K., Ooi, B. S. & Khan, M. Z. M. Tunable self-injection locked green laser diode. *Opt. Lett.* **43**, 4931–4934 (2018).
41. Hult, J., Burns, I. S. & Kaminski, C. F. Wide-bandwidth mode-hop-free tuning of extended-cavity GaN diode lasers. *Appl. Opt.* **44**, 3675–3685 (2005).
42. Schkolnik, V., Fartmann, O. & Krutzik, M. An extended-cavity diode laser at 497 nm for laser cooling and trapping of neutral strontium. *Laser Phys.* **29**, 035802 (2019).
43. Li, C. et al. High-speed multi-pass tunable diode laser absorption spectrometer based on frequency-modulation spectroscopy. *Opt. Express* **26**, 29330–29339 (2018).
44. Riemensberger, J. et al. Massively parallel coherent laser ranging using a soliton microcomb. *Nature* **581**, 164–170 (2020).
45. Idjadi, M. H. & Aflatouni, F. Integrated Pound–Drever–Hall laser stabilization system in silicon. *Nat. Commun.* **8**, 1209 (2017).
46. Spencer, D. T., Davenport, M. L., Komljenovic, T., Srinivasan, S. & Bowers, J. E. Stabilization of heterogeneous silicon lasers using Pound–Drever–Hall locking to Si_3N_4 ring resonators. *Opt. Express* **24**, 13511–13517 (2016).
47. Stéphan, G. M., Tam, T. T., Blin, S., Besnard, P. & Têtu, M. Laser line shape and spectral density of frequency noise. *Phys. Rev. A* **71**, 043809 (2005).

48. Kharas, D. et al. High-power (>300 mW) on-chip laser with passively aligned silicon-nitride waveguide DBR cavity. *IEEE Photonics J.* **12**, 1504612 (2020).
49. Billah, M. R. et al. Hybrid integration of silicon photonics circuits and InP lasers by photonic wire bonding. *Optica* **5**, 876–883 (2018).
50. Nielsen, M. D., Folkenberg, J. R., Mortensen, N. A. & Bjarklev, A. Bandwidth comparison of photonic crystal fibers and conventional single-mode fibers. *Opt. Express* **12**, 430–435 (2004).
51. Hong, S. & Ali, S. Compact arrayed waveguide gratings for visible wavelengths based on silicon nitride. *Ukr. J. Phys. Opt.* **18**, 239 (2017).
52. Andrews, J. R. Enhanced thermal stability of single longitudinal mode coupled cavity lasers. *Appl. Phys. Lett.* **47**, 71–73 (1985).
53. Wieman, C. E. & Hollberg, L. Using diode lasers for atomic physics. *Rev. Sci. Instrum.* **62**, 1–20 (1991).
54. Doret, S. C. Simple, low-noise piezo driver with feed-forward for broad tuning of external cavity diode lasers. *Rev. Sci. Instrum.* **89**, 023102 (2018).
55. Dutta, S., Elliott, D. S. & Chen, Y. P. Mode-hop-free tuning over 135 GHz of external cavity diode lasers without antireflection coating. *Appl. Phys. B* **106**, 629–633 (2012).
56. Spencer, D. T., Bauters, J. F., Heck, M. J. R. & Bowers, J. E. Integrated waveguide coupled Si_3N_4 resonators in the ultrahigh-Q regime. *Optica* **1**, 153–157 (2014).
57. Ji, X. et al. Exploiting ultralow loss multimode waveguides for broadband frequency combs. *Laser Photonics Rev.* **15**, 2000353 (2021).
58. Antman, Y. et al. High power on-chip integrated laser. Preprint at https://arxiv.org/abs/2207.06279 (2022).
59. Siddharth, A. et al. Near ultraviolet photonic integrated lasers based on silicon nitride. *APL Photonics* **7**, 046108 (2022).
60. Petermann, K. *Laser Diode Modulation and Noise* (Springer, 1988).

Methods

Fabrication methods

To fabricate the Si_3N_4 photonic chip, we first grew 1 µm of wet thermal silicon dioxide (SiO_2) on a silicon wafer and deposited 175 nm of Si_3N_4 via low-pressure chemical vapour deposition. Next, we patterned the waveguides and resonators using electron-beam lithography and fluorine-based etching. We clad the devices with 1 µm of SiO_2 via plasma-enhanced chemical vapour deposition. For the microheaters, we used photolithography and a metal lift-off process to pattern 100 nm of platinum on a titanium adhesion layer. Finally, we defined the facets of the photonic chip by etching 150 µm into the silicon substrate using a Bosch etching process, and diced the wafer to separate the individual chip.

Experimental setup

We mounted the FP laser diodes on a six-axis locking kinematic mount (K6XS, Thorlabs), which was placed on a piezo-actuated stage (Tritor 100, Piezosystem Jena) for edge coupling to the photonic chip. To drive the laser diodes we used a power supply (Keithley 2220G-30-1) through an electrostatic-discharge-protection and strain-relief cable (SR9HA, Thorlabs). To drive the microheaters on the chip, we used two separate sources (Keithley 2220G-30-1 for the bus waveguide phase shifter and Keithley 2400 for the resonator phase shifter) through a three-pin electrical probe. We used different cleaved optical fibres (Thorlabs) to collect the chip output for each spectral range (SM450 for near-UV, deep-blue, blue and green wavelengths; SM600 for red wavelengths; and 780HP for near-IR wavelengths). The fibre-coupled light was sent to an optical spectrum analyser (Ando AQ6314A) for spectral measurements and to a wavemeter (Advantest Q8326 for the near-IR range and HighFinesse WSU-10 for the other spectral ranges) for precise wavelength measurements of the self-injection locked lasers. We present detailed descriptions of each experimental measurement in the Supplementary Information.

Data availability

The experimental dataset and its analysis are provided within the paper and its Supplementary Information, and the data are available from the corresponding authors upon reasonable request.

Acknowledgements

This work was supported as part of the Novel Chip-Based Nonlinear Photonic Sources from the Visible to Mid-Infrared funded by the Army Research Office under award no. W911NF2110286. Fabrication of the photonic chips was done in part at the City University of New York Advanced Science Research Center Nanofabrication Facility, in part at the Columbia Nano Initiative Shared Lab Facilities at Columbia University, and in part at the Cornell NanoScale Facility, a member of the National Nanotechnology Coordinated Infrastructure (NNCI), which is supported by the National Science Foundation (Grant NNCI-2025233). M.C.S. is supported by a Facebook Fellowship Award. We thank A. Gaeta, S. Will and his group members M. Kwon and W. Yuan, and T. Zelevinsky and her students Q. Sun and K. H. Leung for lending critical pieces of equipment and for helpful discussions. We also thank U. D. Dave, G. R. Bhatt and Y. Antman for helpful discussions. M.C.-Z. thanks N. Janosik for her support and helpful discussions.

Author contributions

M.C.-Z. conceived the chip-scale visible lasers research project. M.C.-Z., A.G.-M. and A.M. had the initial discussions that shaped the first steps and goals of the project. With helpful suggestions from A.G.-M., M.C.-Z. designed the photonic devices and experiments. M.C.-Z., X.J. and M.C.S. fabricated the photonic chips. M.C.-Z. and A.M. performed experiments on some preliminary devices. M.C.-Z. performed the experimental measurements and analysed the results, with crucial suggestions from A.G.-M. along the way. M.C.-Z. prepared the manuscript. X.J., A.G.-M., M.C.S., A.M. and M.L. edited the manuscript. M.L. supervised the project.

Competing interests

M.C.-Z., A.G.-M, X.J., M.C.S., A.M. and M.L. are named inventors on US provisional patent application 63/275,141 regarding the technology reported in this article.

Additional information

Supplementary information The online version contains supplementary material available at https://doi.org/10.1038/s41566-022-01120-w.

Correspondence and requests for materials should be addressed to Mateus Corato-Zanarella or Michal Lipson.

Peer review information *Nature Photonics* thanks the anonymous reviewers for their contribution to the peer review of this work.